Optimal Path Planning for Helical Gear Profile Inspection with Point Laser Triangulation Probes

Kevin B. Smith
Professor,
Brigham Young University,
Dept. of Electrical and Computer Engineering,
Provo, UT 84602

Yuan F. Zheng
Professor,
The Ohio State University,
Dept. of Electrical Engineering,
Columbus, OH 43210

New commercial Point Laser Triangulation (PLT) probes enable Coordinate Measuring Machines (CMMs) to take faster, noncontact, accurate measurements. In this paper, we address how to apply this technology to inspect helical gears. Traditionally, gears are inspected with slow, costly, and dedicated machines. The proposed flexible inspection system with a fast measuring probe can significantly reduce capital equipment costs and inspection times. Integrating PLT probes on CMMs has been limited partly because of the difficulty in generating optimal inspection paths, and partly because of the highly reflective gear surfaces. Complex sensor-to-surface orientation and obstacle-avoidance requirements of these unique probes are the main cause of the difficulty. This paper presents a geometrical approach for obtaining an optimal path plan for helical gear profile inspection with PLT probes. Models for the orientation parameters and the allowable operating regions for the PLT probe are developed. A collision avoidance strategy is also presented. Although this new method was developed and demonstrated while creating an optimal path plan for inspecting helical gears, the developed models and principles can also be applied to optimal inspection plan generation for other parts.
[DOI: 10.1115/1.1349718]

1 Introduction

The profile inspection of helical gears has traditionally been performed with dedicated gear inspection equipment. This equipment is expensive, slow, and inflexible for inspecting various gear types and other products. More recently, gears are being inspected with Coordinate Measuring Machines [1]. The CMM requires very little setup time, and can accurately measure a large range of gear sizes. In addition, noncontact inspection methods are being proposed to speed up the process.

Tansel [2] proposed a noncontact method for inspecting the miniature gears by evaluating the intensity variation of reflected laser from the tooth surfaces while rotating.

A dedicated optical gear measuring system for measuring pitch errors and tooth profiles was developed by E. Okuyama et al. [3]. The advantage of this approach is high-speed measurements. The disadvantage is the lack of flexibility of the equipment to measure other parts or other dimensions.

S. Wu and G. Lu [4] apply phase-shift optical triangulation technique to gear profile measurement. In this technique, a surface patch is measured while the gear and sensor are held in a fixed position. Currently, the system requires a master gear for comparative analysis.

In a cooperative effort, McVea and Mellis [1] demonstrated that a Coordinate Measuring Machine (CMM) with a contact probe can be used confidently to control bevel gear accuracy and consistency. Their work illustrated the flexible nature of a CMM: they obtained measurements of tooth form, tooth size, run-out, and pitch variation, which formerly were obtained from dedicated inspections machines [5].

Previous works have used point lasers triangulation probes for digitizing (inspecting) arbitrary, high-dimension sculpture surfaces, but were never applied to helical gears. Although the gear surface appears less arbitrary and has lower dimensions than a sculptured surface, the protruding teeth of a helical gear and the dimension and physical shape of the laser sensor attached to the CMM are not a natural match. It is extremely difficult to position the laser sensor so that it not only avoids collision but also produces the highest inspection accuracy. This paper provides a solution, for the first time, to optimal path planning of noncontact laser sensors for inspecting helical gears.

In our work, the CMM is enhanced by replacing the traditional touch probe with a PLT probe. This has the added benefit of speeding up the inspection process. However, the PLT probe has a much smaller range of allowable sensor-to-surface orientations than does a touch probe [6]. The allowable orientations are specified by the probe manufacturer, and are determined by the probe's performance while varying surface reflectivity properties and orientations. The added orientation constraint complicates planning the probe's inspection path. We address the problem of how to simplify the generation of this inspection path.

The setup for the proposed noncontact profile measurement of a helical gear is shown in Fig. 1. The helical gear is mounted on a rotary table with the axis of rotation of the gear and rotary table coincident and parallel with the z axis. The angular position of the rotary table is continuous. The touch probe is used to localize the gear. Work by Sahoo and Menq [7] presents methods for part localization of complex surfaces, which is critical for the accurate correlation of measure points to an idealized model. Both the touch probe and the PLT probe are positioned with a two-axes indexable head. Techniques for extrinsic calibration of a PLT probe to a CMM are studied in [8]. The indexable head can be indexed to only a finite number of positions. The time required to index the indexable head and rotate the rotary table is assumed to be much greater than the time required for the CMM to move the x, y, and z axes to a new location.

Solving the path-planning task involves selecting the indexed position of the head and the angular rotation, ω, such that it minimizes the overall required inspection time while maintaining the sensor-to-surface orientation in the allowable region and avoiding collisions. To do this, the inspection points on the gear must be known as a function of gear rotation, ω. The set of possible indexed positions, the allowable region of the PLT probe, and the collision-free region must also be known. The inspection time is reduced by minimizing the number of indexed positions of the probe head that must be used and by minimizing the motion of the rotary table. This is based on the assumption that the probe head

Contributed by the Manufacturing Engineering Division for publication in the JOURNAL OF MANUFACTURING SCIENCE AND ENGINEERING. Manuscript received July 1999; revised Feb. 2000. Associate Editor: J. Lee.

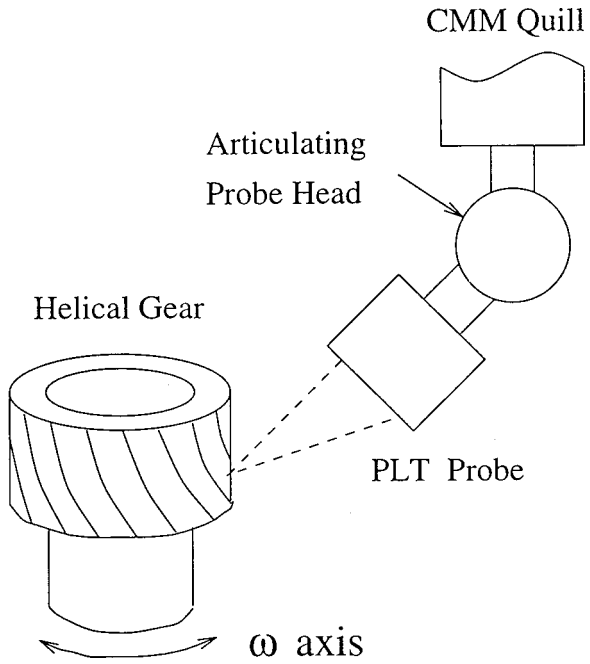

Fig. 1 Setup for proposed noncontact profile gear inspection

typically takes 2.5 seconds to index, and rotary index tables for metrology inspection typically take 2 to 4 seconds to index between 10 deg to 120 deg. CMMs with a touch trigger probe typically take 1 second per measurement, but if the CMM has scanning capability, the sample time for a PLT probe is reduced to a few milliseconds per measurement.

The process of obtaining an optimal inspection path is as follows. First, the points to measure and the corresponding surface normal vectors must be determined as a function of the angular position. The profile inspection points and normal vectors for an involute gear are shown (dots and vectors respectively) in Fig. 2. Note that the density of the points measured along the profile is only limited by the probe's and the CMM's resolution. Once the points are measured, surfaces and curves can be fit to the data and used to identify differences between the measured and ideal geometry. Next, the allowable region of the PLT probe is mapped to each inspection point (see cone in Fig. 2). These are the allowable sensor-to-surface orientations where the PLT probe measurement error is below an acceptable value. A collision-free subspace of the allowable region is determined based on the geometry of the gear and PLT probe (see unshaded position of cone in Fig. 2). This collision-free allowable region is a function of gear rotation, ω.

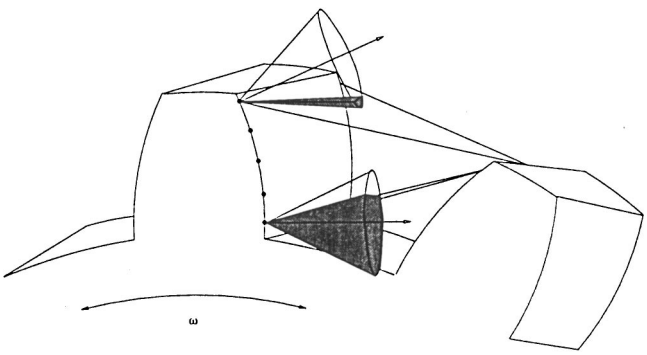

Fig. 2 Collision regions (shaded area) restrict the allowable region to provide allowable and collision-free subspace

At this point, the inspection points, the normal vectors, and the collision-free allowable regions are known as functions of the rotary angle, ω. Also, a set of head-indexed positions are available to choose from. From the restricted allowable region and available indexed positions, an optimal inspection path that minimizes the overall inspection time must be determined.

The rest of the paper is organized as follows. The general concepts of the optimal path-planning method are presented first. They are followed by a flowchart of the program used to implement the optimal path-planning method. The subsequent four sections present the details needed to implement the method, such as calculating the profile inspection points and normals, explaining and defining the orientation parameter space that affects accuracy, and explaining the collision-avoidance strategy. The results of applying the optimal path-planning method to a typical helical gear are also presented. The paper concludes with a summary.

2 Optimal Path-Planning Concept

The task of finding the optimal inspection path is accomplished by evaluating the set of points that can be inspected and the corresponding optimal inspection paths for each available index position. The set of optimal inspection paths is then evaluated to determine a minimal set of indexed positions that can be used to inspect all points and that will minimize the overall inspection time.

The optimal inspection path for a given indexed position is determined by the following process. For each indexed position and each inspection point, the set of angular values of ω_k where the inspection point can be measured with the PLT probe in the collision-free allowable region is determined. These values of ω_k are described by a pair of variables, v_{ik} and ρ_{ik}, where i is the indexed position, and k is the k^{th} inspection point. The allowable values of ω_k are assumed to be continuous, and are bounded by

$$v_{ik}-\rho_{ik}\leqslant\omega_k\leqslant v_{ik}+\rho_{ik}. \tag{1}$$

An illustration of a set of these piecewise, continuous, allowable ω_k values for a given indexed position is shown as vertical lines in Fig. 3. The average ω_k value over the contiguous values is v_{ik}; the range of contiguous values of ω_k is ρ_{ik}. If all the allowable ω_k values for a given indexed position are not contiguous, then a unique v_{jk} and ρ_{jk} pair can be defined for each contiguous section and treated as if they came from a different indexed position.

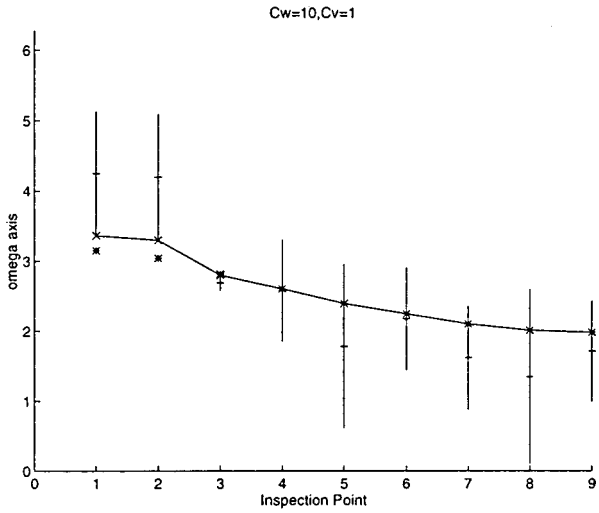

Fig. 3 Optimal path using weights $C_\omega=10$, $C_v=1$, where |=Allowable angles (ω_k); −=Center angles (v_{ik}); *=Optimal angles (ω_k^*); and ×=Clipped angles ($\hat{\omega}_k$)

The optimal path for an indexed position is determined by minimizing the required gear rotation between inspection points (i.e., $(\omega_{ik}-\omega_{ik-1})^2$), and by minimizing the difference between the ω_{ik} value and v_{ik} overall inspection points (i.e., $k=1$ to q). Thus, the cost function for the desired minimization is

$$J_i=\left(\sum_{k=1}^{q} C_\omega(\omega_k-\omega_{k-1})^2+C_v(\omega_k-v_{k-1})^2\right)_i, \tag{2}$$

where C_ω and C_v are constant weights, $\omega_0=\omega_1$, and $\omega_{q+1}=\omega_q$. The first term in the summation provides a weighted cost for rotating the gear between inspection points. This is desirable because the rotation of the gear is assumed slow compared to positioning the PLT probe with the CMM. The second term provides a weighted cost for the inspection point being off-center in the allowable gear rotation region. This cost is desirable to position the PLT probe clear of the forbidden regions.

For finding the minimum of J, one takes the partial derivative of J with respect to ω_k and sets the result equal to zero:

$$\frac{\partial J_i}{\partial \omega_k}=\left(\left(-2-\frac{C_v}{C_\omega}\right)\omega_k-\omega_{k-1}-\omega_{k+1}-v_k\frac{C_v}{C_\omega}\right)_i. \tag{3}$$

Writing this set of equations in matrix form produces

$$\underbrace{\begin{bmatrix} \gamma+1 & 1 & 0 & 0 & 0 & \cdots & 0 \\ 1 & \gamma & 1 & 0 & 0 & \cdots & 0 \\ 0 & 1 & \gamma & 1 & 0 & \cdots & 0 \\ \vdots & \ddots & \ddots & \ddots & \ddots & \ddots & \vdots \\ 0 & \cdots & 0 & 1 & \gamma & 1 & 0 \\ 0 & \cdots & 0 & 0 & 1 & \gamma & 1 \\ 0 & \cdots & 0 & 0 & 0 & 1 & \gamma+1 \end{bmatrix}}_{A} \underbrace{\begin{bmatrix} \omega_1 \\ \omega_2 \\ \vdots \\ \omega_q \end{bmatrix}}_{\omega^*} = -\frac{C_\omega}{C_v}\underbrace{\begin{bmatrix} v_1 \\ v_2 \\ \vdots \\ v_q \end{bmatrix}}_{z}, \tag{4}$$

where $\gamma=-2-C_v/C_\omega$. The solution to the optimal rotary angles, ω_k^*, is

$$\boldsymbol{\omega}^*=A^{-1}\mathbf{z}. \tag{5}$$

Because the ω_k^* values are bounded by ρ_k, if $|\omega_k^*|>|v_k+\rho_k|$, then ω_k^* must be clipped to the maximum allowable value. An equation to accomplish this clipping is

$$\acute{\omega}_k=v_k+sign(\omega_k^*-v_k)\min(\rho,|\omega_k^*-v_k|), \tag{6}$$

where $\acute{\omega}_k$ is the clipped values and the *sign*() function returns the algebraic sign of its argument.

To illustrate this optimal path-planning technique, random values for v_k and ρ_k were generated and the optimal $\acute{\omega}_k$ was calculated as described above. The weights C_ω and C_v were varied in the plots to demonstrate their effect on the optimal path. The results are plotted in Figs. 3 and 4.

Figure 3 demonstrates that if $C_v/C_\omega<1$, the optimal path will tend toward a constant ω value. Figure 4 demonstrates that if $C_v/C_\omega>1$, the optimal path will have ω_k values that tend toward values of v_k.

The overall optimal path is determined from the minimal set of index positions required to inspect all points, and that require the minimal amount of motion of the rotary table during the inspection.

3 Optimal Path-Planning Implementation

The proposed optimal path-planning technique for measuring the profile helical gear with a PLT probe was implemented using Matlab script files. The basic flowchart for the implementation is shown in Fig. 5. At the start, the program is initialized with the specifications for inspection of the helical gear. After initialization, the program has a series of ''for loops'' to vary parameters, such as the tooth being inspected, the indexed position, and gear-axis rotation. In the main section of the program, the inspection points, the allowable region, and the collision-free region are all

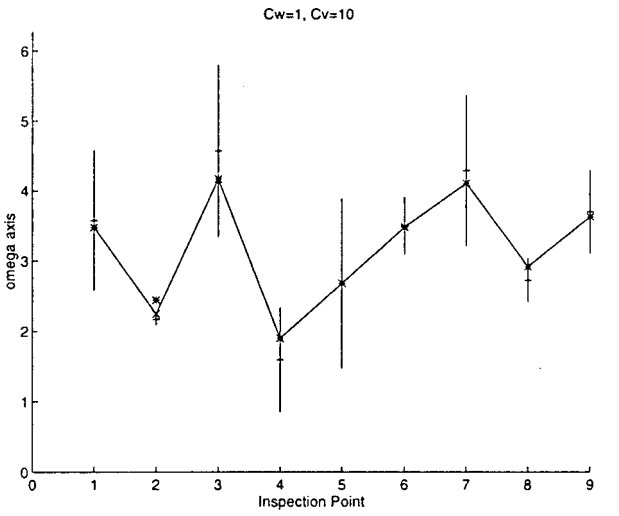

Fig. 4 Optimal path using weights $C_\omega=1$, $C_v=10$

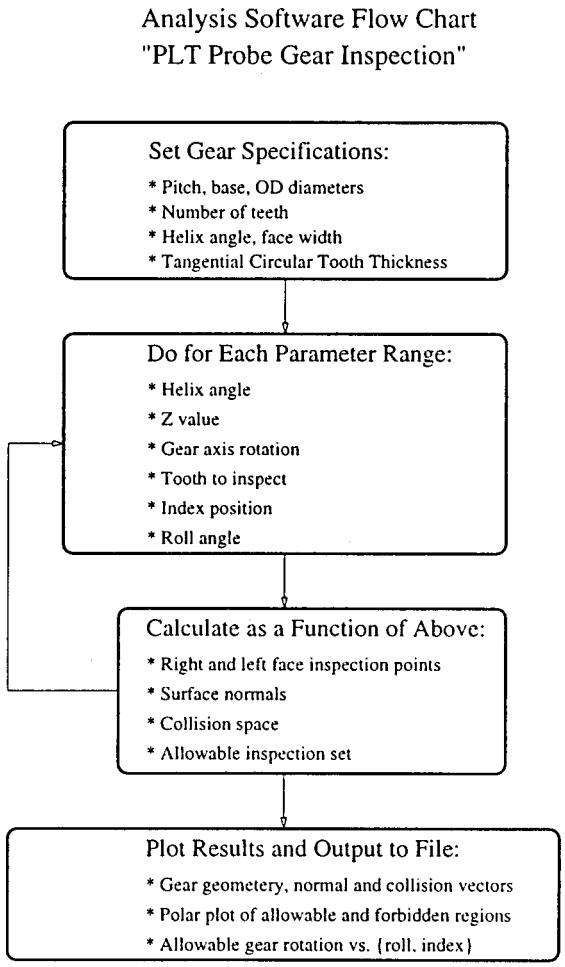

Fig. 5 Optimal path-planning flowchart for profile inspection of helical gears using a PLT probe

calculated. The program outputs plots that show gear geometry, allowable and collision regions, and allowable ω values versus inspection-point position.

These main areas of the program are discussed below.

4 Helical and Involute Curve Parameters

The tooth profile of a helical gear in the transverse plane (i.e., perpendicular to the axis of rotation) is an involute curve. Because of symmetry, the variables used in the program to construct the involute curves are referenced from the center of the tooth (see Figs. 6 and 7). The angle, α_o, from the *x*-axis to the center of the tooth is calculated by

$$\alpha_o = \alpha_k + \psi_z + \omega, \tag{7}$$

where α_k is the angle to tooth number k referenced from tooth number 1, ψ_z is the tooth rotation from a reference z axis height due to the helix angle, and ω is the angular rotation of the rotary table. The angle, α_k, is determined by

$$\alpha_k = \frac{-2\pi\left(k - \frac{1}{2}\right)}{N}. \tag{8}$$

From this equation, the zero reference position is found to be centered between tooth number 1 and tooth number N. The teeth are numbered clockwise when viewing the gear's axial reference surface.

The tooth rotation (or twist), ψ_z, as a function of displacement, Δz, along the gear axis and the helix angle, ψ, is

$$\psi_z = \frac{\Delta z \tan(\psi)}{\frac{D_c}{2}}, \tag{9}$$

where D_c is the diameter where the tooth thickness is specified (typically, the pitch diameter).

The angle β_o (see Fig. 8) is measured from the center of the tooth to the point on the base circle where the profile begins (i.e., roll angle $\beta = 0$), and is calculated by

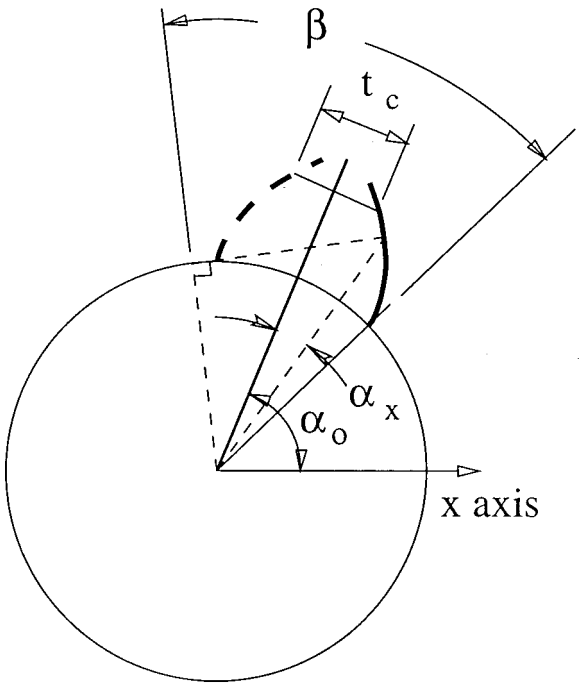

Fig. 6 Involute construction variables for right-tooth profile

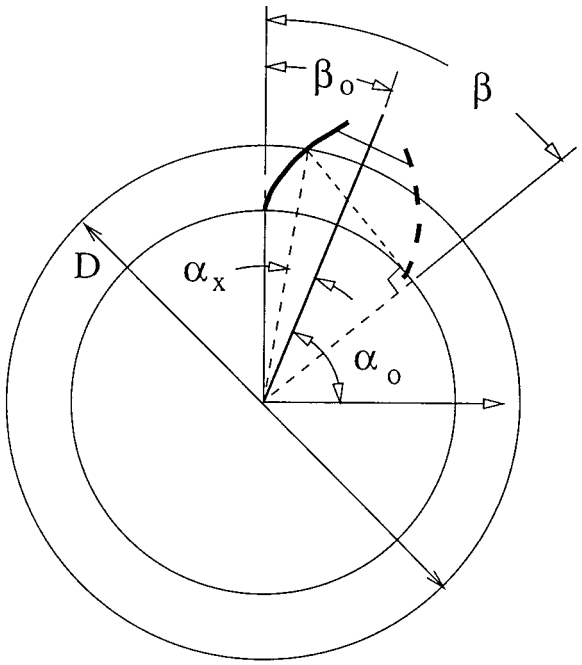

Fig. 7 Involute construction variables for left-tooth profile

$$\beta_o = \beta_c + \alpha_c - \phi_c. \tag{10}$$

The variables β_c, α_c, and ϕ_c will be derived by first expressing the diameter, D, on the involute curve as a function of the roll angle. The diameter, D, on a profile created with a base circle diameter, D_b, at a roll angle, β (in radians), is given by

$$D = D_b\sqrt{1+\beta^2}. \tag{11}$$

Rearranging and solving for β, the roll angle for the profile at a diameter, D, gives

$$\beta = \sqrt{\left(\frac{D}{D_b}\right)^2 - 1}. \tag{12}$$

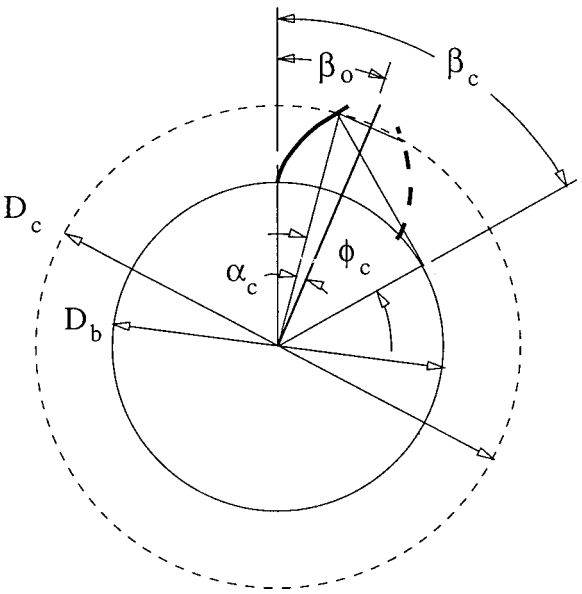

Fig. 8 The angle β_o, measured from the tooth center to roll angle of zero location on the base circle

Using this result, roll angle β_c, shown in Fig. 8, is given by

$$\beta_c = \sqrt{\left(\frac{D_c}{D_b}\right)^2 - 1}. \tag{13}$$

From right triangles, the angle α_c is

$$\alpha_c = \sin^{-1}\left(\frac{t_c}{2D_c}\right), \tag{14}$$

and the angle ϕ_c is

$$\phi_c = \tan^{-1}\left(\frac{D_b\beta_c}{D_b}\right) = \tan^{-1}(\beta_c). \tag{15}$$

The segment of the profile curve to be inspected is bounded by the starting roll angle, β_s, and the ending roll angle, β_e. From (12), these roll angles are calculated from their corresponding starting diameter, D_s, and ending diameter, D_e:

$$\beta_s = \sqrt{\left(\frac{D_s}{D_b}\right)^2 - 1}, \tag{16}$$

$$\beta_e = \sqrt{\left(\frac{D_e}{D_b}\right)^2 - 1}. \tag{17}$$

The points on the tooth profile are found from the magnitude and angle of a vector from the center of the gear rotation to the profile point in the transverse plane. The magnitude of the vector is given by (11). The angle of the vector from the *x*-axis is the sum of the angle, α_o, to the center of the tooth plus the angle, α_x, from the center of the tooth to desired point (see Fig. 6). The angle α_x is given by

$$\alpha_x = \beta_o - (\beta - \tan^{-1}(\beta)). \tag{18}$$

Combining these two results, points on the involute in the transverse plane as a function of the roll angle are given by

$$r_x = \frac{D_b}{2}\sqrt{1+\beta^2}\cos(\alpha_o - \Gamma\alpha_x), \tag{19}$$

$$r_y = \frac{D_b}{2}\sqrt{1+\beta^2}\sin(\alpha_o - \Gamma\alpha_x), \tag{20}$$

$$r_z = z_o + \Delta z, \tag{21}$$

where

$$\Gamma = \begin{cases} +1, & \text{for the right tooth face} \\ -1, & \text{for the left tooth face} \end{cases}. \tag{22}$$

The *z*-axis value of the transverse plane, as shown, is the sum of the starting, or reference, *z*-axis value, z_o, plus an offset, Δz.

The tangent vector, $\mathbf{t}_\beta$, to the profile curve is obtained through the partial derivative of (19) to (21) with respect to β. The result is

$$t_{\beta x} = \frac{(\cos(\alpha_o) - \Gamma\beta\sin(\alpha_o))}{\sqrt{1+\beta^2}}, \tag{23}$$

$$t_{\beta y} = \frac{(\Gamma\beta\cos(\alpha_o) + \sin(\alpha_o))}{\sqrt{1+\beta^2}}, \tag{24}$$

$$t_{\beta z} = 0. \tag{25}$$

The tangent to the helix curve, $\mathbf{t}_\psi$, (i.e., moving along the tooth face at a constant diameter) is found by taking the partial derivative of (19) to (21) with respect to *z*. The result is

$$t_{\psi x} = \frac{-D_b\tan(\psi)}{\sqrt{D_b^2\tan^2(\psi) + R_c^2(1+\beta^2)}} \tag{26}$$

$$\times\sin(\alpha_o - \Gamma\alpha_x), \tag{27}$$

$$t_{\psi y} = \frac{D_b\tan(\psi)}{\sqrt{D_b^2\tan^2(\psi) + R_c^2(1+\beta^2)}} \tag{28}$$

$$\times\cos(\alpha_o - \Gamma\alpha_x), \tag{29}$$

$$t_{\psi z} = \frac{D_c(1+\beta^2)}{\sqrt{D_b^2\tan^2(\psi) + R_c^2(1+\beta^2)}}. \tag{30}$$

The normal to the tooth surface, **n**, is found by taking the cross-product of the tangent, $\mathbf{t}_\beta$, to the profile curve with the tangent, $\mathbf{t}_\psi$, to the helical curve:

$$\mathbf{n} = \mathbf{t}_\beta \times \mathbf{t}_\psi. \tag{31}$$

Using this information, each inspection point is described by its position (see (19) to (21)) and its normal vector (see (31)), which are both functions of the roll angle. The tangent to the helix curve, $\mathbf{t}_\psi$, will be used later to define collision planes.

5 Orientation Parameters Affecting Accuracy

The accuracy of the PLT probe is significantly affected by its orientation to the surface normal vector [6]. There are two orientation parameters, both of which are angles found to affect the accuracy of a PLT probe. One of the orientation parameters is the angle of incidence, α, of the laser beam with the workpiece surface (i.e., the angle between the surface normal vector and the laser beam), calculated from the tooth surface normal vector, **n**, and the PLT probe approach vector, **a**, by using the dot product of the vectors:

$$\alpha = \cos^{-1}(-\mathbf{n}\cdot\mathbf{a}). \tag{32}$$

The other orientation parameter, ϕ, describes the position of the PLT probe orientation vector, **o**, relative to the surface normal (see Fig. 9). It is the angle using the right-hand-rule about the approach vector from the incident angle plane to the triangulation plane. To find the angle, ϕ, a vector, **q**, is constructed so that the angle between the orientation vector, **o**, and **q** is ϕ.

The constraints on **q** to yield this result are that (1) **q** is in the plane containing the vectors **a** and **n**; i.e., $(\mathbf{a}\times\mathbf{n})\cdot\mathbf{q}=0$; (2) **q** is orthogonal to **a**; i.e., $\mathbf{q}\cdot\mathbf{a}=0$; (3) **q** is in the ''direction'' of **n**; i.e., $\mathbf{n}\cdot\mathbf{q}>0$; and (4) **q** is a unit vector; i.e., $\mathbf{q}^T\cdot\mathbf{q}=1$. An equation for $\acute{\mathbf{q}}$ that satisfies constraints (1) and (2) is given by

$$\acute{\mathbf{q}} = (\mathbf{a}\times\mathbf{n})\times\mathbf{a}. \tag{33}$$

From $\acute{\mathbf{q}}$, constraints (3) and (4) can be met and **q** constructed using the equation

$$\mathbf{q} = sign(\acute{\mathbf{q}}\cdot\mathbf{n})\frac{\acute{\mathbf{q}}}{|\acute{\mathbf{q}}|}. \tag{34}$$

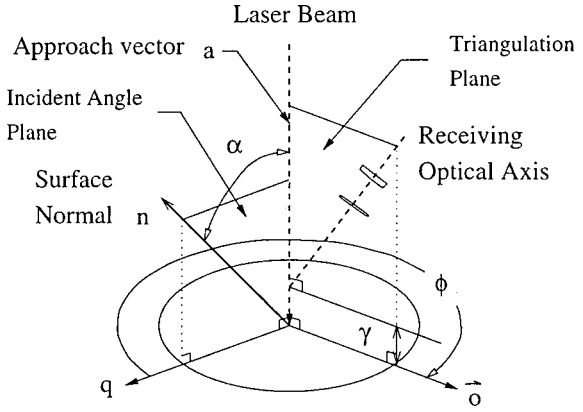

Fig. 9 Orientation parameters, α, ϕ, and γ, for a PLT probe

Finally, the angle ϕ, between vectors **q** and **o**, rotating about vector **a** where **q** and **o** are both perpendicular to **a** is

$$\phi = sign((\mathbf{q}\times\mathbf{o})\cdot\mathbf{a})\cos^{-1}(\mathbf{o}\cdot\mathbf{q}). \quad (35)$$

Once the orientation parameters, α and ϕ, are known for a given surface normal, **n**, at a location to inspect, the orientation parameters can be used to determine the expected accuracy of the PLT probe measurement. If the expected accuracy is better than the desired accuracy, the point can be measured. If the expected accuracy is worse than the desired accuracy, the sensor-to-surface orientation must be changed to a position where the expected accuracy is within the desired limit. The process for making this determination will now be presented.

6 Allowable Orientation Region

From the orientation parameters and the displacement measurement value, γ, a three-dimensional allowable orientation region can be constructed. This region specifies values of orientation parameter triplets (α,ϕ,γ) where the expected measurement error, γ_{err}, is below a desired limit. The set of all possible triplets can be denoted by

$$S_T = \{(\alpha,\phi,\gamma): 0 \leqslant \alpha < \pi, 0 \leqslant \phi < 2\pi, \gamma_{\min} \leqslant \gamma \leqslant \gamma_{\max}\}. \quad (36)$$

The allowable region, a subset of S_T, is denoted by $S_A \subseteq S_T$. The forbidden region is the complement of allowable region, denoted by $S_F = \mathbf{S}_A$. The allowable region can be plotted using a polar plot for a given value of γ or range of γ where the plot is constant (see Fig. 10). Points in the region are defined by vectors where the magnitude of the vector is the angle α and the angle that the vector makes with the horizontal axis is ϕ. Since the angle of a vector is cyclic quantity with a period of 2π, the entire possible region mapped by α and ϕ is contained within a circle with a radius of π. The allowable region within this larger region is known to be bounded by a circle with a radius of $\pi/2$, if the measured surface is assumed to approximate a plane locally and is not transparent. From here, the allowable region is best determined experimentally by performance evaluation testing for a particular PLT probe.

There are typically three orientation regions where a PLT probe performs poorly. These regions are called forbidden regions. The first is the region where α approaches $\pi/2$ and $|\phi| \leqslant \pi - \epsilon$. The value of ϵ is determined experimentally. This region corresponds to the laser beam being parallel to the workpiece surface. The second region is where $|\phi|$ approaches π and α approaches $\pi/2 - \theta$. The angle θ is the angle in the triangulation plane between the laser beam and the optical axis of the receiving lens. In this case, the optical axis of the receiving lens becomes co-planar with the inspection surface. The third region is where α approaches $\theta/2$ and ϕ approaches 0. In this region, the surface normal is half-way between the laser beam and the optical axis of the receiving lens. In this orientation, specular reflection from the surface is viewed by the detector biasing the centroid location of the resulting spot, which results in significant measurement errors.

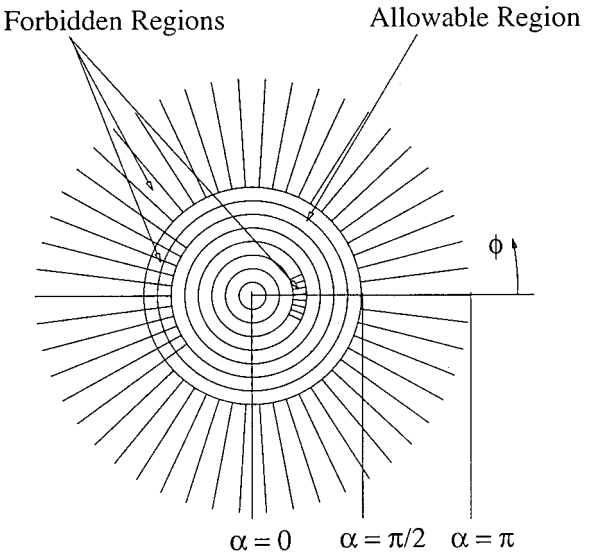

Fig. 10 Plot of allowable regions (circular lines) and forbidden regions (radial lines) for a typical PLT probe

In the path-planning program, these three regions were described using bounding values for α and ϕ. The PLT probe is defined to be in the first forbidden region if $\alpha > \alpha_{1\,\max}$. It is defined to be in the second forbidden region if $|\phi| > \phi_{2\,\max}$ and $\alpha > \alpha_{2\,\max}$. The third forbidden region is defined by $|\phi| < \phi_{3\,\min}$ and $\alpha_{3\,\max} < \alpha < \alpha_{3\,\min}$. Once the bounding values are known, a pair of orientation parameter values can be checked quickly using simple if-then logic statements to determine if the PLT probe is being operated in the allowable region.

As shown above, the map from the vectors **n**, **a**, and **o** to the orientation parameters, α and ϕ, is unique. The converse map, however, is not unique. Rotating the vectors **a** and **o** about the vector **n** does not change the corresponding orientation parameters, α and ϕ. Thus an α and ϕ point in the allowable region corresponds to an infinite set of **a** and **o** vectors that are all symmetric about the normal vector **n**. Thus, an allowable region in α, ϕ space corresponds to a much larger allowable region for the vectors **a** and **o**.

7 Collision Avoidance Strategy

The strategy used to avoid collisions in this undertaking is to construct two collision planes per inspection point that identify areas the PLT probe should not enter. The collision planes are defined to pass through the inspection point, and have normal vectors, $\mathbf{n}_{ci}$, for $i = 1,2$. The first collision normal vector, $\mathbf{n}_{c1}$, is equal to the normal vector of the tooth surface in (31). That is, it defines a plane parallel to the surface being measured. The second collision normal vector will be defined below.

A collision is detected (or defined to occur) when the angle of incidence (32) between the approach vector and the collision plane is ''too'' large and surface is within the measuring range of the probe. (i.e., γ is within its allowable range). Thus, the collision-free area for the approach vector forms a cone around the normal vector of collision plane. We will now formally define the approach and extend it both to collision planes and to using the optical axis as follows.

For a specified PLT probe position (i.e., **a** and **o** are known), a collision is defined to occur with collision plane i when

$$-\mathbf{a}\cdot\mathbf{n}_{ci} \leqslant C_{ai\,\max}. \quad (37)$$

where $C_{ai\,\max} > 0$.

Also compared is the angle between collision normal vectors and the vector along the optical axis of the receiving lens. A vector along the optical axis of the receiving lens is found by taking the difference between the orientation vector and the approach vector. A collision is also defined to occur when

$$(C_{ol}\mathbf{o} - \mathbf{a})\cdot\mathbf{n}_{ci} \leqslant C_{oi\,\max}, \quad (38)$$

where $C_{oi\,\max} > 0$ and C_{ol} is the distance from the laser beam to the optical axis of the receiving lens. The specific values for $C_{ai\,\max}$, $C_{oi\,\max}$, and C_{ol} are determined from the geometry of the PLT probe.

The second collision normal vector, $\mathbf{n}_{c2}$, is defined so that the PLT probe does not collide with or is obstructed by an adjacent tooth. The collision normal vector, $\mathbf{n}_{c2}$, is constructed using the geometry of the helical gear (see Fig. 11). The normal vector, $\mathbf{n}_{c2}$, is derived from

$$\mathbf{n}_{c2} = \mathbf{t}_{\psi}\times(\mathbf{h}_c - \mathbf{r}), \quad (39)$$

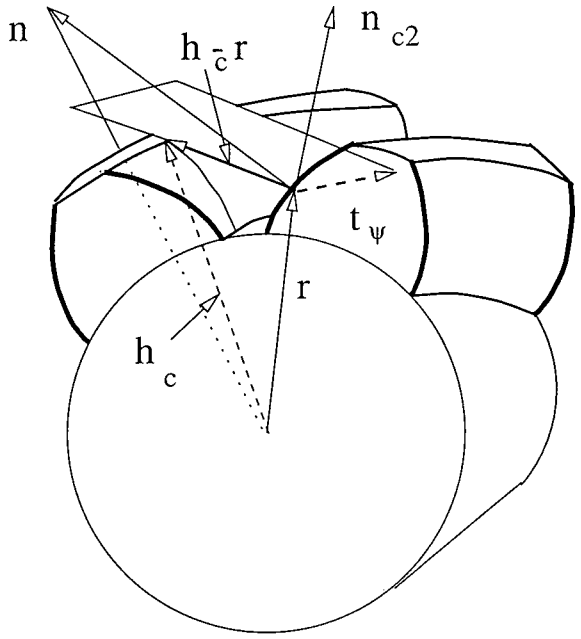

Fig. 11 The vector h_c is on the O.D. helical curve of the facing adjacent tooth, and is in the transverse plane defined by vectors r and n. The collision plane normal n_{c2} is defined as $n_{c2} = t_\psi \times (h_c - r)$

where $\mathbf{t}_\psi$ is the tangent vector on the tooth's face in the axial direction, and $\mathbf{h}_c$ is a vector from the measured point to a point on the opposite tooth in the normal plane, where collision occurs on the outside diameter (OD) of the tooth.

Two equations are used to solve for $\mathbf{h}_c$. One comes from the equation of the adjacent O.D. helical curve. This helical curve equation, written as a function of ψ_z, is

$$h_c x(\psi_z) = \frac{D_o}{2}\cos(\acute{\alpha}_k - \Gamma\,\delta\alpha_k + \Gamma\,\delta\alpha_x + \psi_z), \tag{40}$$

$$h_c y(\psi_z) = \frac{D_o}{2}\sin(\acute{\alpha}_k - \Gamma\,\delta\alpha_k + \Gamma\,\delta\alpha_x + \psi_z), \tag{41}$$

$$h_c z(\psi_z) = z_o + \frac{D_c \psi_z}{\tan(\psi)}, \tag{42}$$

where $\acute{\alpha}_k$ is the angle to the center of the tooth being inspected, $\delta\alpha_k = 2\pi/N$ (i.e., the angle between two adjacent teeth), and $\delta\alpha_x$ is the angle measured in the transverse plane from the center of the adjacent tooth to the helical curve that $\mathbf{h}_c$ is on. This angle, $\delta\alpha_x$, is given by

$$\delta\alpha_x = \beta_o - (\beta_{od} - \tan^{-1}(\beta_{od})), \tag{43}$$

where

$$\beta_{od} = \sqrt{\frac{D_o^2}{D_b^2} - 1}. \tag{44}$$

The second equation needed to solve for $\mathbf{h}_c$ is obtained by using the constraint that the vectors $\mathbf{r}$, $\mathbf{n}$, and $\mathbf{h}_c$ are co-planar in the normal plane. This provides the relation that

$$\mathbf{h}_c \cdot (\mathbf{r} \times \mathbf{n}) = 0. \tag{45}$$

Carrying out the cross-product and substituting in (40) to (42) yields

$$A\cos(\acute{\alpha}_k - \Gamma\,\delta\alpha_k + \Gamma\,\delta\alpha_x + \psi_z) + B\sin(\acute{\alpha}_k - \Gamma\,\delta\alpha_k + \Gamma\,\delta\alpha_x + \psi_z) + C\psi = D, \tag{46}$$

where

$$A = (r_y n_z - r_z n_y)\frac{D_o}{2}, \tag{47}$$

$$B = (r_z n_x - r_x n_z)\frac{D_o}{2}, \tag{48}$$

$$C = (r_x n_y - r_y n_x) D_c / (2\tan(\psi)), \tag{49}$$

$$D = (r_x n_y - r_y n_x) z. \tag{50}$$

Because (46) is nonlinear, solving for ψ_z requires an iterative approach, such as a Newton's method for solving equations. Once ψ_z is obtained, the vector $\mathbf{h}$ can be found from (40) to (42). Knowing $\mathbf{h}_c$, the normal vector n_{c2} for the second collision plane is found from (39).

With the collision planes defined, optimal path-planning can be implemented.

8 Optimal Path-Planning Experiment

The optimal path-planning method described above for helical gear profile inspection was applied to a typical helical gear. The specifications of the gear needed to calculate the profile inspection points are shown in Table 1.

The profile inspection points generated by the program for eight sections of the tooth for both left and right sides of the tooth, and for three teeth are shown in Figs. 12 and 13. Also shown are the normal vectors, $\mathbf{n}$, and collision vectors, $\mathbf{h}_c - \mathbf{r}$, for one left and right profile.

Table 1 Helical gear specifications required to calculate the profile inspection points

Name	Value	Description
N	30	Number of teeth
D_o	135.432	Outside diameter (mm)
D_b	119.342	Base circle diameter (mm)
D_r	114.755	Root diameter (mm)
D_c	127.000	Chordal diameter(mm)
t	6.548	T.C. tooth thickness (mm)
F_o	22.100	Axial face width (mm)
ψ	30°	Helix angle on D_c

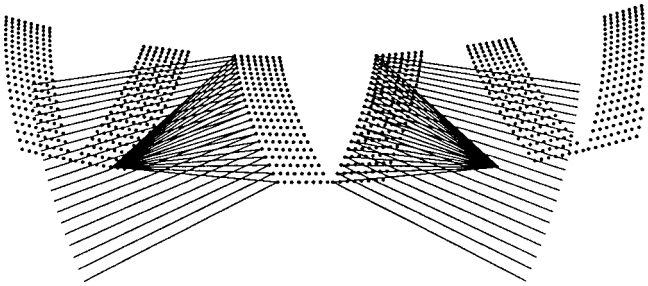

Fig. 12 Top view of the calculated profile inspection points, normal vectors, and collision vectors (i.e., $h_c - r$)

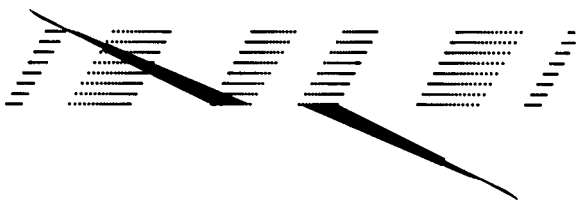

Fig. 13 Front view of the calculated profile inspection points, normal vectors, and collision vectors (i.e., $h_c - r$)

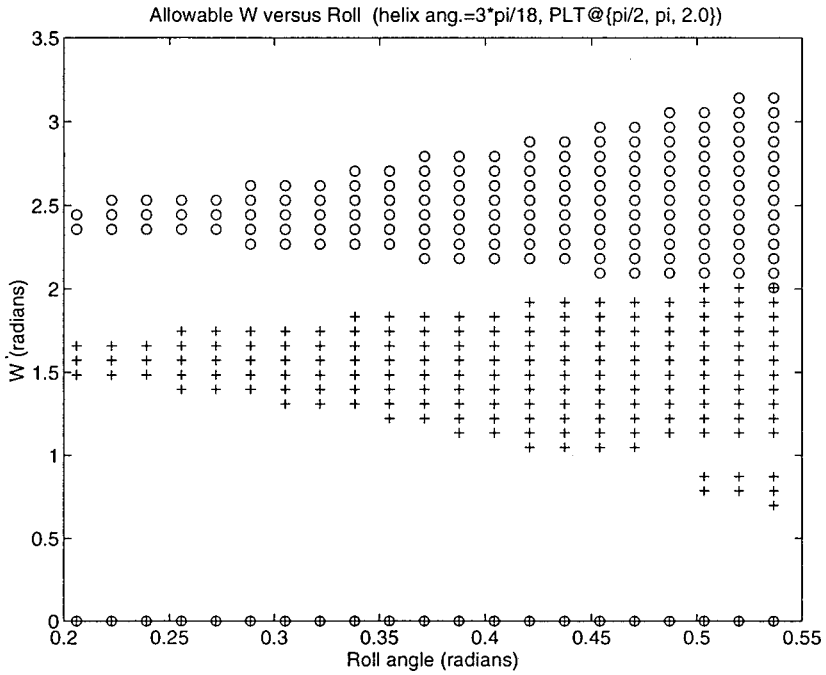

Fig. 14 ω value versus roll angle providing profile inspection in the allowable and collision-free region where ○=right tooth ω values; +=left tooth ω values; a={−1,0,0}; and o={0.000,0.909,−0.416}

The allowable collision-free values of ω as a function of the roll angle are plotted below for inspection of the profile curve of the helical gear specified in Table 1.

In Fig. 14, the ω values are plotted for an indexed position with approach vector $\mathbf{a}=\{-1,0,0\}$, and orientation vector $\mathbf{o}=\{0.000,0.909,-0.416\}$. As shown, the PLT probe can accurately measure without collision all inspection points (i.e., all roll angles) on both the left and right tooth faces. The optimal path for this indexed position consists of ω being a constant during inspection of a tooth. From the figure, the optimal ω value is 2.4 radians for inspecting the right tooth and 1.6 radians for inspecting the left tooth.

In Fig. 15, the ω values are plotted for an indexed position, resulting in $\mathbf{a}=\{-1,0,0\}$, $\mathbf{o}=\{0.000,0.500,0.866\}$. This indexed position orients the PLT probe so that both the left and right sides of the tooth can again be measured accurately and without collision.

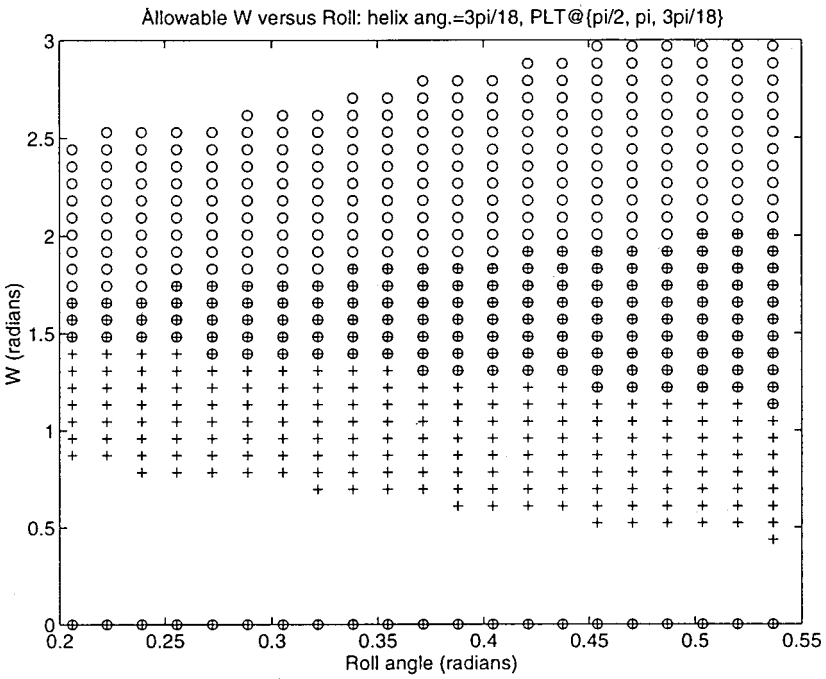

Fig. 15 ω value versus roll angle providing profile inspection in the allowable and collision-free region, where ○=right tooth ω values; +=left tooth ω values; a={−1,0,0}; and o={0.000,0.500,0.866}

However, the plot shows that a single ω value of 1.6 radians allows both the left and right tooth faces to be measured using a single indexed position. Thus this single indexed position and constant ω provide an overall optimal path for inspecting the helical gear with a PLT probe.

9 Summary

This paper outlined the objectives of implementing a new optimal path-planning technique for inspecting the profile of a helical gear and described how these objectives were met. The technique successfully minimized the overall profile inspection time by finding the minimum set of index positions and the minimum required movement of the rotary table during the inspection process. The complexities of the helical profile curves, allowable regions, and collision regions were handled by first deriving equations for each as a function of the roll angle and angular position of the rotary table. Next, the angular positions were determined for each indexed position that allowed the profile points to be measured accurately by the PLT probe while avoiding collision. Collision avoidance was partially accomplished by defining collision planes, which proved to be very effective and simple to implement. Finally, an optimal path for finding ω as a function of roll angle that minimizes inspection time was presented and demonstrated.

This research was funded in part by the Engineering Research Center for Net Shape Manufacturing (ERC/NSM) at The Ohio State University, by the Office of Naval Research under grant N00014-90-J1516, and by the National Institute of Standards and Technology (NIST), an agency of the U.S. Department of Commerce.

Nomenclature

ω = rotary table angle
ω_k = rotary table angles for a measured point
υ_{ik} = mean value of ω_k
ρ_{ik} = range of ω_k
J_i = cost function
C_ω = cost function weights
C_υ = cost function weights
$\boldsymbol{\omega}^*$ = optimal rotary angles
$\acute{\omega}_k$ = clipped optimal rotary angles
α_o = angle from the x-axis to tooth center
α_k = angle between reference tooth and tooth number k
ψ_z = tooth rotation due to helix angle
Δz = displacement along the gear axis
D_c = diameter where the tooth thickness is specified
β = roll angle for profile at diameter D
β_o = angle measured from tooth center
D = the diameter on the involute curve
β_s = start roll angle
D_s = starting roll diameter
β_e = ending roll angle
D_e = ending roll diameter
$\mathbf{r}$ = point on the involute
$\mathbf{t}_\beta$ = tangent vector to the profile curve
$\mathbf{t}_\psi$ = tangent vector to the helix curve
$\mathbf{n}$ = normal vector to the tooth surface
$\mathbf{a}$ = approach vector of PLT probe
ϕ = orientation parameter
$\mathbf{o}$ = orientation vector
γ = measured displacement value
S_T = set of all possible orientations
S_A = allowable region
S_F = forbidden region
$\mathbf{n}_c$ = collision plane normal vector

References

[1] McVea, W. R., and Mellis, D. W., 1991, ''Spiral Bevel Tooth Topography Control Using CMM Equipment,'' SAE Trans., **100**, pp. 121–134.
[2] Tansel, I., Li, W., Carballo, M., Trujillo, M., Fallerio, B., and Paz, E., 1994, ''High-speed Micro Gear Inspection by Evaluating Laser Beam Reflections,'' *ASME Press Series on International Advances in Design Productivity. Artificial Neural Networks in Engineering Conference*, **4**, pp. 987–992, Nov.
[3] Okuyama, E., Kiyono, S., and Moritoki, H., 1994, ''Investigation of an Optical Noncontact Gear Geometry Measurement System: Measurement of Pitch Errors and Tooth Profiles,'' Precis. Eng., **16**, No. 2, pp. 117–123, Apr.
[4] Wu, S., and Lu, G., 1998, ''Non-Contact, High-Speed, Precision Gear Inspection,'' *Annual Forum Proceedings—American Helicopter Society Proceedings 54th Annual Forum. Part 2*, **2**, pp. 701–711, May.
[5] AGMA, ''Gear Classification and Inspection Handbook for Unassembled Spur and Helical Gears,'' 1988, *American Gear Manufacturers Association*, ANSI/AGMA 2000-A88, Mar.
[6] Smith, K. B., and Zheng, Y. F., 1998, ''Accuracy Analysis of Point Laser Triangulation Probes Using Simulation,'' ASME J. Manuf. Sci. Eng., **120**, No. 4, pp. 736–745.
[7] Sahoo, K. C., and Menq, C. H., 1991, ''Localization of 3-D Objects Having Complex Sculptured Surfaces Using Tactile Sensing and Surface Description,'' ASME J. Eng. Ind. **523**, pp. 85–92, Feb.
[8] Smith, K. B., and Zheng, Y. F., 1999, ''Point Laser Triangulation Probe Calibration for Coordinate Metrology,'' ASME J. Manuf. Sci. Eng., in press.